

RESEARCH

Open Access



Differential cardiomyocyte transcriptomic remodeling during in vitro *Trypanosoma cruzi* infection using laboratory strains provides implications on pathogenic host responses

Katherine-Sofia Candray-Medina^{1,2,3}, Yu Nakagama^{1,2*} , Masamichi Ito^{4,5}, Shun Nakagama⁶, Evariste Tshibangu-Kabamba^{1,2,7}, Norihiko Takeda⁸, Yuki Sugiura⁹, Yuko Nitahara^{1,2}, Yu Michimuko-Nagahara^{1,2}, Natsuko Kaku^{1,2}, Yoko Onizuka¹⁰, Carmen-Elena Arias³, Maricela Mejia³, Karla Alas³, Susana Peña¹¹, Yasuhiro Maejima⁶, Issei Komuro^{12,13}, Junko Nakajima-Shimada¹⁰ and Yasutoshi Kido^{1,2}

Abstract

Background Chagas disease can lead to life-threatening cardiac manifestations. Regional factors, including genetic characteristics of circulating *Trypanosoma cruzi* (*T. cruzi*), have attracted attention as likely determinants of Chagas disease phenotypic expression and Chagas cardiomyopathy (CCM) progression. Our objective was to elucidate the differential transcriptomic signatures of cardiomyocytes resulting from infection with genetically discrete *T. cruzi* strains and explore their relationships with CCM pathogenesis and progression.

Methods HL-1 rodent cardiomyocytes were infected with *T. cruzi* trypomastigotes of the Colombian, Y, or Tulahuen strain. RNA was serially isolated post-infection for microarray analysis. Enrichment analyses of differentially expressed genes (fold-change ≥ 2 or ≤ 0.5) highlighted over-represented biological pathways. Intracellular levels of reactive oxygen species (ROS) were compared between *T. cruzi*-infected and non-infected HL-1 cardiomyocytes.

Results We found that oxidative stress-related gene ontology terms (GO terms), 'Hypertrophy model', 'Apoptosis', and 'MAPK signaling' pathways (all with $P < 0.01$) were upregulated. 'Glutathione and one-carbon metabolism' pathway, and 'Cellular nitrogen compound metabolic process' GO term (all with $P < 0.001$) were upregulated exclusively in the cardiomyocytes infected with the Colombian/Y strains. Mean intracellular levels of ROS were significantly higher in the *T. cruzi*-infected cardiomyocytes compared to the non-infected ($P < 0.0001$).

Conclusions The upregulation of oxidative stress-related and hypertrophic pathways constitutes the universal hallmarks of the cardiomyocyte response elicited by *T. cruzi* infection. Nitrogen metabolism upregulation and glutathione metabolism imbalance may implicate a relationship between nitrosative stress and poor oxygen radicals scavenging in the unique pathophysiology of Chagas cardiomyopathy.

Keywords *Trypanosoma cruzi*, Chagas disease, Transcriptome, HL-1, In vitro modeling, Dilated cardiomyopathy, Glutathione metabolism, Oxidative stress, Neglected tropical diseases

*Correspondence:

Yu Nakagama

ynakagama@gmail.com; nakagama.yu@omu.ac.jp

Full list of author information is available at the end of the article



© The Author(s) 2023. **Open Access** This article is licensed under a Creative Commons Attribution 4.0 International License, which permits use, sharing, adaptation, distribution and reproduction in any medium or format, as long as you give appropriate credit to the original author(s) and the source, provide a link to the Creative Commons licence, and indicate if changes were made. The images or other third party material in this article are included in the article's Creative Commons licence, unless indicated otherwise in a credit line to the material. If material is not included in the article's Creative Commons licence and your intended use is not permitted by statutory regulation or exceeds the permitted use, you will need to obtain permission directly from the copyright holder. To view a copy of this licence, visit <http://creativecommons.org/licenses/by/4.0/>.

Introduction

Chagas disease, caused by *Trypanosoma cruzi* (*T. cruzi*) protozoan infection, affects more than 6 million people worldwide, with more than 70 million people at risk of infection [1–3]. In the absence of curative treatment, approximately 30% of those chronically infected will present Chagas cardiomyopathy (CCM) as a phenotypic outcome. CCM is a life-threatening condition characterized by myocardial dilatation, conduction abnormalities, and heart failure [4]. The molecular pathophysiology and indicators of CCM progression have been least described among other common forms of dilated cardiomyopathy, such as those related to ischemic/hypoxic stress (mitochondrial dysfunction and impaired calcium sensitivity of cardiomyocytes) or viral infections (viral RNA persistence and subsequent apoptotic loss of cardiomyocyte) [5–15].

The diverse genetic make-up of parasite virulence factors shall evoke unique host responses of variable magnitude [16–21], collectively affecting the phenotypic expression of CCM. Thus, the host response to specific *T. cruzi* genotypes may provide clues to the molecular pathophysiology of CCM progression [22–24]. The objective of the current study was to elucidate the transcriptomic signatures of the cardiomyocyte response to infection with genetically discrete *T. cruzi* strains namely, Colombian, Y, and Tulahuen to explore differential host responses and their relationships with CCM pathogenesis and progression.

Materials and methods

Cell lines and culture conditions

Mouse CH3/10T1/2, clone 8 murine fibroblasts (RRID: CVCL_0190, JCRB0003), obtained from the Japanese Collection of Research Bioresources Cell Bank (JCRB), were cultured in high-glucose Dulbecco's modified DMEM medium (Fujifilm, Japan) supplemented with 10% fetal bovine serum and 1% penicillin/streptomycin (Fujifilm, Osaka, Japan). The cells were seeded in T-25 vent-cap flasks and incubated at 37 °C, under 5% CO₂.

Mouse HL-1 cardiomyocytes (RRID: CVCL_0303) were cultured in Claycomb medium (Merck, Darmstadt, Germany) supplemented with 10% fetal bovine serum (Gibco, Maryland, USA), 0.1 mM norepinephrine (Sigma), 0.2 mM L-glutamine (Fujifilm, Osaka, Japan), and 1% penicillin/streptomycin (Fujifilm, Osaka, Japan). Cells were seeded on T-25 vent-cap flasks pre-coated with fibronectin (Sigma, St. Louis, MO, USA) and incubated at 37 °C, under 5% CO₂.

T. cruzi epimastigotes of the Colombian, Y, and Tulahuen strains were obtained from NEKKEN Bio-Resource Center (NBRC) and cultured in LIT medium at 28 °C,

under 5% CO₂. Per strain, 1 × 10⁸ epimastigotes harvested in the exponential growth phase were subjected to metacyclogenesis, following a pre-established protocol [25]. Debris sedimentation was performed by centrifugation at 700 ×g for 5 min followed by trypomastigote collection of the supernatant at 1700 ×g for 10 min. Trypomastigotes were used to infect CH3/10T1/2 cells at a multiplicity of infection (MOI) 1:10. After 5–7 days, successful infection was confirmed by the presence of intracellular amastigotes on light microscopy. Cultured cell-derived trypomastigotes (CCdT), obtained from the supernatant of these stable cultures under the aforementioned centrifugation condition, were used for cardiomyocyte infection experiments.

In vitro cardiomyocyte infection

The 6-well plates were seeded with HL-1 cardiomyocytes as described previously and incubated for 24 h to ensure full attachment and confluency. CCdT of each strain was collected to infect HL-1 cardiomyocytes at an MOI of 10:1. Mouse TNF-α (100 ng/mL; Sigma-Aldrich H8916, Missouri, USA) was added to the culture medium of the positive control wells [19, 21, 26–31]. CCdT were allowed to interact with the HL-1 cells for 24 or 48 h depending on the intended condition and were not washed during this interaction period. Non-infected conditions for both 24 and 48 h time points were prepared separately to control for unexpected changes during time course. Each condition was prepared in duplicates.

Assessment of trypanosome infectivity by light microscopy

At 24- and 48-h post-infection (hpi), cells were fixed and stained with Diff-Quick solution (Sysmex, Kobe, Japan). For each cardiomyocyte infection condition, 'percentage of infected cells', as well as the 'intracellular amastigote count per infected cell', were determined by light microscopy to serve as surrogates of the strains infectivity rate. Eight microscopic fields were counted after staining. The results are representative of two separately performed experiments. Pairwise comparisons were performed with the Mann–Whitney test.

Microarray analysis of differentially expressed genes (DEGs)

At 24 and 48 hpi, the culture medium was removed, and cells were gently washed with sterile PBS. Total RNA was isolated using the NucleoSpin RNA kit (Macherey–Nagel, Düren, Germany), according to the manufacturer's instructions. RNA concentration and purity were assessed using Nanodrop 2000 (ThermoFisher, Wilmington, USA). RNA samples were analyzed using the Clariom S Assay for Mouse (Applied BioSystems, CA, USA) microarray platform to identify DEGs.

Data analysis was done on the Microarray Data Analysis Tool software version 3.2.0.0 (Filgen, Nagoya, Japan). Background signal was defined as any signal intensity values below the median of the signal intensity of a set of negative control probes on the microarray. The threshold for background level was determined as 43 for the infected conditions and 48 for the negative control at 24 hpi; 52 for the infected conditions and 48 for the negative control at 48 hpi. Valid gene probes were the set of probes which surpassed these thresholds of intensity in every infection condition at each time point. Probes not fulfilling the criteria were considered invalid and excluded. Therefore, 11,041 and 11,000 valid gene probes for each respective time point were included for further analyses. Fold change (FC) was defined as the ratio between gene expression level of the infected conditions (or the positive control) and the negative control. *P*-value (*P*) was calculated by the 'Student's t-test' to determine the significance of FC of a gene per comparison. Multiple comparison-adjusted *P*-values were estimated by the Benjamini–Hochberg method using GraphPad Prism version 9.5.1 for Windows (GraphPad Software, Massachusetts, USA). $FC \geq 2$ or ≤ 0.5 , and $P < 0.05$ were used as the threshold to define DEGs.

FC of the valid genes shared across all cardiomyocyte infection conditions (total 10,784 genes) were used as input for the principal component analysis (PCA). Analysis and plotting were performed with R 4.1.0 software, and the 'FactoMineR' and 'Factoextra' R packages [32–34]. The principal components 1 and 2, which together described 58.9% of the total variance in the dataset, were selected to plot the PCA results.

Pathway and gene ontology enrichment analysis

Pathway and gene ontology (GO) category analysis was performed using the Microarray Data Analysis Tool software version 3.2.0.0 (Filgen, Nagoya, Japan). Pathways were enriched using the WikiPathways system [35].

Enrichment of both pathways and GO categories was performed using the gene sets (common to all three strains, or selectively shared between Colombian and Y strains) of upregulated and downregulated DEGs as input. The *P*-value for each pathway and GO category was calculated using the two-tailed Fisher's exact test. Significantly (Z -score (Z) > 0 , $P < 0.01$) enriched pathways and the top GO terms (up to ten, in the order of lowest *P*) were selected for discussion. Bar plots depicting GO and pathway enrichment were generated using the 'GOplot' R package [36].

Assessment of reactive oxygen species (ROS) intracellular content

The 96-well plates were seeded to a 50% confluency with HL-1 cardiomyocytes as described previously and incubated for 24 h to ensure full attachment. CCdT of *T. cruzi* Y strain were used to infect HL-1 cardiomyocytes at an MOI of 10:1. Each condition was performed in triplicates. After 24 h, sterile PBS was used to wash non-internalized parasites. Cells were incubated with CellRox green (ThermoFisher, Wilmington, USA) at 10 μ M for 30 min, then, gently washed and counterstained with Hoechst dye solution (Abcam, Cambridge, UK) at 4 μ M for 15 min. Image acquisition was performed with a BZ-X700 series Keyence microscope (Keyence, Osaka, Japan). Image analyses were performed with the ImageJ software (National Institute of Health, USA) [37]. For each biological replicate, four cell images were randomly chosen to measure their fluorescence intensity for the CellRox green probe, and three random background measurements were also performed. Background fluorescence was subtracted from the cell measurements to calculate the cell fluorescence. Mann–Whitney test was used for group comparisons.

Results

Assessment of infectivity by strain

At 24 hpi, Colombian, Y and Tulahuen infections showed 37.2%, 45.1%, and 17.2% infected cardiomyocytes, respectively (Fig. 1, left). A similar trend persisted at 48 hpi when the infected cardiomyocytes counted 70.5%, 85.2%, and 26.0% for Colombian, Y and Tulahuen infections, respectively (Fig. 1, right). At 24 hpi, each infected cell contained a mean (standard deviation): 1.6 (0.8), 1.6 (0.9), and 1.2 (0.4) intracellular amastigotes for Colombian-, Y-, and Tulahuen-infected conditions, respectively. A similar trend in differential infectivity persisted at 48 hpi, showing intracellular amastigote counts of 2.8 (1.9), 3.3 (1.8), and 2.1 (1.6) per Colombian, Y, and Tulahuen strain-infected cells, respectively. Pairwise comparisons found significant differences between Colombian and Y against Tulahuen strain ($P < 0.01$), in both 24 and 48 hpi. Distribution and exact *P* values are depicted in Fig. 2. A representative image from each infection condition is depicted in Additional file 2: Fig. S1.

Host transcriptomic remodeling per infecting *T. cruzi* strain

In the Colombian-, Y-, and Tulahuen 24-h-infected conditions, 1097 (4.9%), 1122 (5.1%), and 806 (3.6%) DEGs were identified. 32 DEGs were identified in the TNF- α -treated control condition (Additional file 2: Fig. S2). The proportions of up- and down-regulated DEGs per

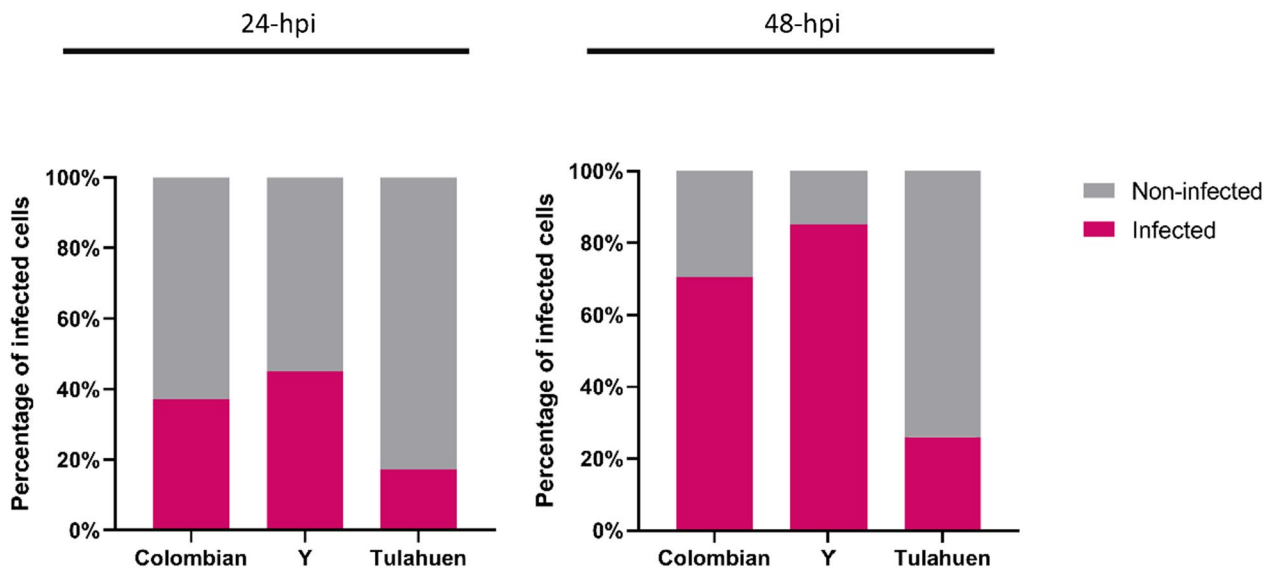


Fig. 1 Difference in cardiomyocyte infectivity among *Trypanosoma cruzi* infection conditions. Percentage of *T. cruzi*-infected cells (containing intracellular amastigotes) at 24- and 48-h post-infection. *hpi* hours post-infection

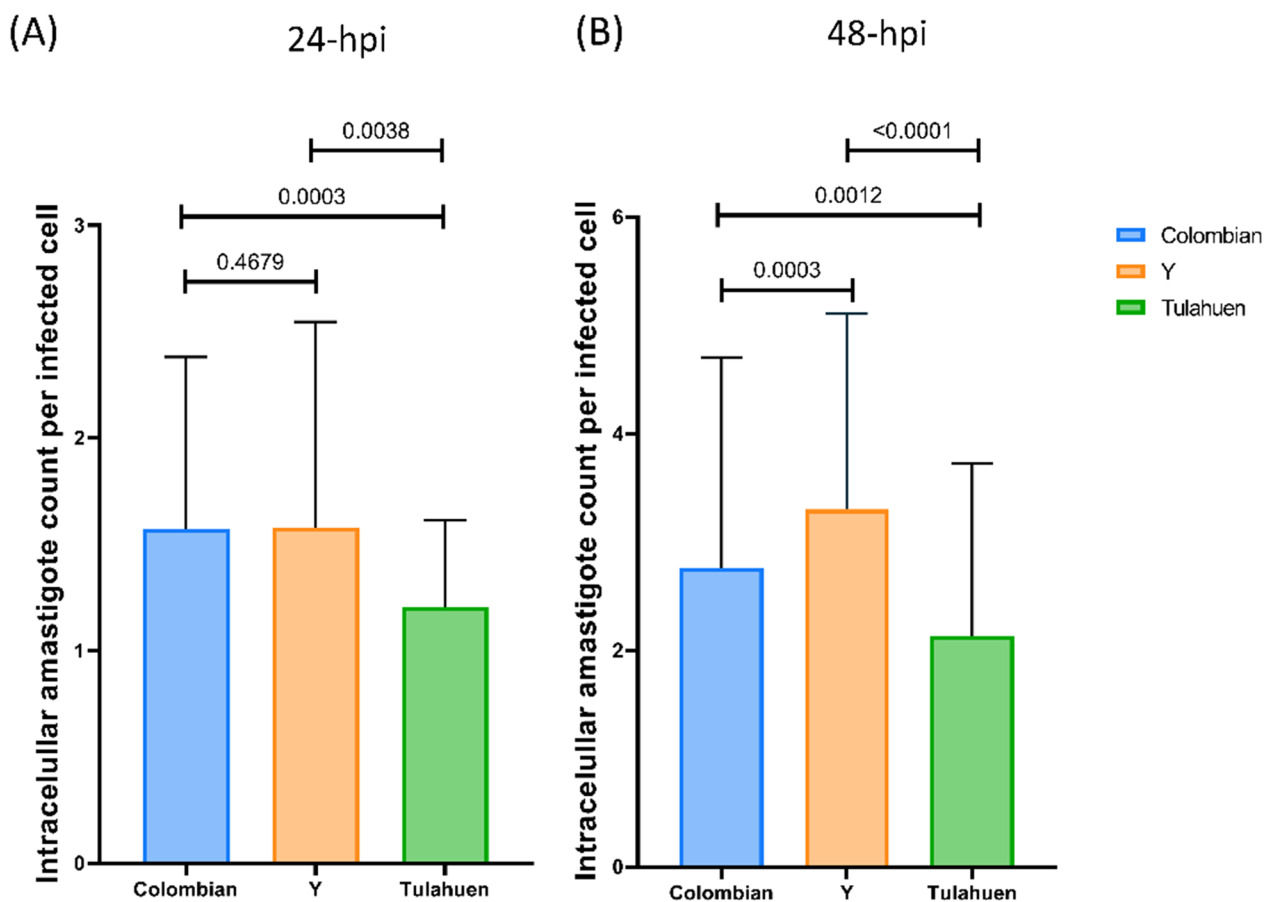
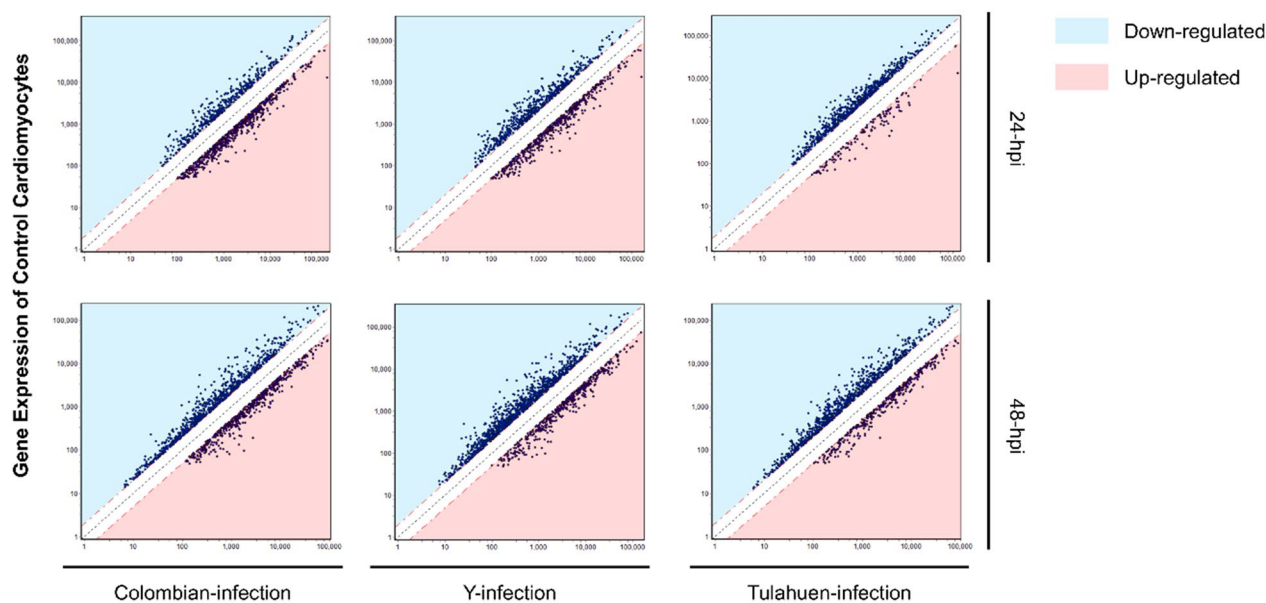


Fig. 2 Cardiomyocyte infectivity among different *Trypanosoma cruzi* infection conditions. Intracellular amastigote counts per infected cell are plotted at **A** 24- and **B** 48-h post-infection. Pairwise comparisons were performed with Mann-Whitney test. Black horizontal bars indicate the mean and SD



Gene Expression of Chagas Disease-model Cardiomyocytes

Fig. 3 Remodeling of gene expression profiles in cardiomyocytes infected with three different *Trypanosoma cruzi* strains at two time points post-infection. Y axes indicate the gene expression level of the non-infected control cardiomyocyte, while X-axes indicate gene expression levels of *Trypanosoma cruzi*-infected cardiomyocytes. The black dashed line, and upper and lower red dashed lines show the line of identity, and the 0.5- and twofold change thresholds, respectively. Each plot represents a differentially expressed gene (DEG). Blue and pink shaded areas represent down- and up-regulated DEGs, respectively. hpi hours post-infection

cardiomyocyte infection condition are depicted in Fig. 3. Colombian and Y infections led to increased numbers of upregulated DEGs at 24 hpi. A similar trend persisted at 48 hpi but to a lesser extent. At 24 hpi, a significant overlap of upregulated DEGs (438 of 666 (66%) in Colombian-, or of 538 (81%) in Y-infection) was observed between Colombian and Y infection, of which 107 (24%) were also shared with Tulahuen-infection (Fig. 4A). Uniquely in Tulahuen-infection, downregulated genes over-represented the total DEGs at 24 hpi. A large proportion of downregulated DEGs (315 of 431 (73%) in Colombian-, 584 (54%) in Y-, and 684 (46%) in Tulahuen-infection) were shared among all infection conditions, suggesting a common pathway of cardiomyocyte functional deterioration (Fig. 4B). As apparent in the PCA plot, the Colombian- and Y-infection conditions were more closely related in terms of the gene expression pattern (Fig. 5), potentially reflecting the significant overlap of upregulated DEGs between the strains and the distinctive over-representation of downregulated DEG in Tulahuen-infection. At 24 hpi, the three infection conditions showed more discrete host cardiomyocyte gene expression patterns compared at 48 hpi. This indicated that 24 hpi would serve as a more favorable time frame to investigate the uniqueness of the host transcriptional

remodeling triggered by each infecting *T. cruzi* strain. Not only were we more interested in the earlier determinants of CCM progression, but the PCA findings also supported our selection of the 24-hpi stage of the in vitro cardiomyocyte infection model as the main focus of the following analyses.

The common cardiomyocyte response to *T. cruzi* infection

Of the 107 commonly upregulated genes, eight had $FC \geq 5$. The top upregulated genes were Arresting Domain Containing 4 (*Arrdc4*), thioredoxin interacting protein (*Txnip*), and growth differentiation factor 15 (*Gdf15*). (Fig. 6 A).

The 107 upregulated DEGs shared among all three infection conditions enriched pathways related to 'Hypertrophy model' ($Z=7.90$, $P<0.001$), 'Apoptosis' ($Z=4.8$, $P<0.01$), 'Aminoacid metabolism' ($Z=4.3$, $P<0.01$), 'MAPK signaling pathway' ($Z=3.9$, $P<0.01$), 'ErbB signaling pathway' ($Z=4.9$, $P<0.01$), 'Spinal cord injury' ($Z=4.2$, $P<0.01$), 'Selenium metabolism-selenoproteins' ($Z=4.8$, $P<0.01$), and 'Homologous recombination' ($Z=6.5$, $P<0.01$) (Fig. 7A). The same gene list was enriched in genes associated with the Biological Process GO terms of 'Response to reactive oxygen species' ($Z=8.1$, $P<0.001$), 'Response to ionizing radiation'

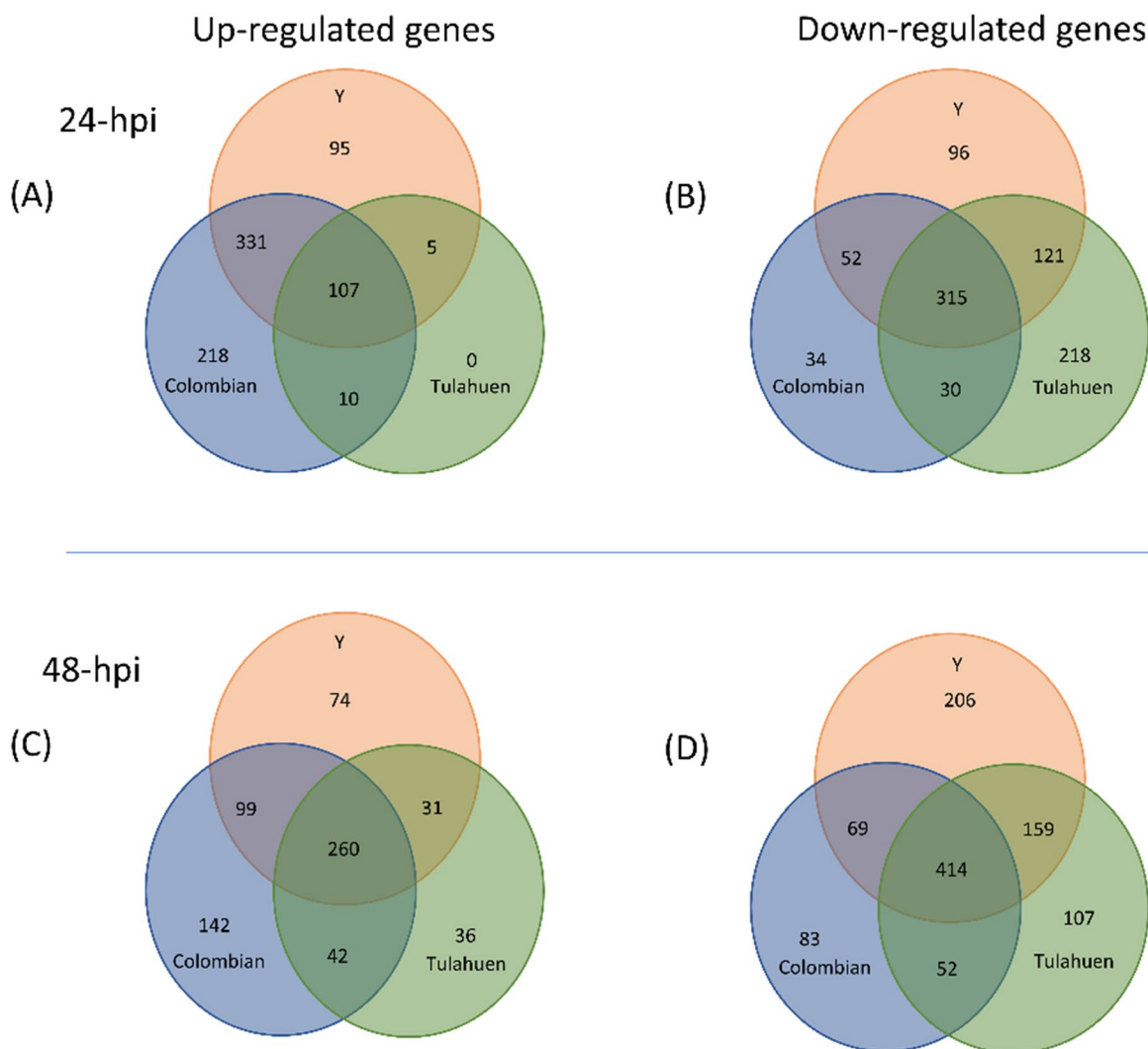


Fig. 4 Identification of differentially expressed genes (DEGs) of the host cardiomyocyte upon *Trypanosoma cruzi* infection. Numbers of up- (left column) and down-regulated (right column) DEGs at 24- (upper row) and 48-h post-infection (lower row) are shown in the respective Venn diagrams. *hpi* hours post-infection

($Z=8.2$, $P<0.001$), 'Response to oxidative stress' ($Z=6.7$, $P<0.001$), 'Response to hydrogen peroxide' ($Z=8.1$, $P<0.001$), 'Cellular response to stress' ($Z=5.3$, $P<0.001$), 'Primary metabolic process' ($Z=3.3$, $P<0.001$), 'Regulation of metabolic process' ($Z=3.9$, $P<0.001$), and 'Regulation of intracellular protein kinase cascade' ($Z=5.4$, $P<0.001$) (Fig. 7C).

Of the 315 commonly downregulated genes, 14 had an $FC \leq 0.2$ (Fig. 6B). The 315 downregulated DEGs shared among all three infection conditions enriched pathways related to 'Cholesterol metabolism' ($Z=16.8$, $P<0.001$), 'Cholesterol biosynthesis' ($Z=16.1$, $P<0.001$), 'Integrin-mediated cell adhesion' ($Z=4.2$, $P<0.01$), 'Apoptosis' ($Z=4.3$, $P<0.01$), 'p53 signaling' ($Z=4.2$, $P<0.01$),

'SREBF and miR33 in cholesterol and lipid homeostasis' ($Z=5.3$, $P<0.01$) and 'Omega-9 FA synthesis' ($Z=4.8$, $P<0.01$) (Fig. 7B). The same gene list was enriched in genes associated with the Biological Process GO terms of 'Sterol biosynthetic process' ($Z=17.9$, $P<0.001$), 'Cholesterol biosynthetic process' ($Z=16.5$, $P<0.001$), 'Sterol metabolic process' ($Z=12.9$, $P<0.001$), 'Cholesterol metabolic process' ($Z=11.8$, $P<0.001$), 'Cytoskeleton organization' ($Z=7.9$, $P<0.001$), 'Cellular component organization' ($Z=6.0$, $P<0.001$), 'Steroid biosynthetic process' ($Z=10.5$, $P<0.001$), 'Cellular component organization or biogenesis' ($Z=5.9$, $P<0.001$), 'Actin cytoskeleton organization' ($Z=8.1$, $P<0.001$), and 'Alcohol biosynthetic process' ($Z=10.0$, $P<0.001$) (Fig. 7D).

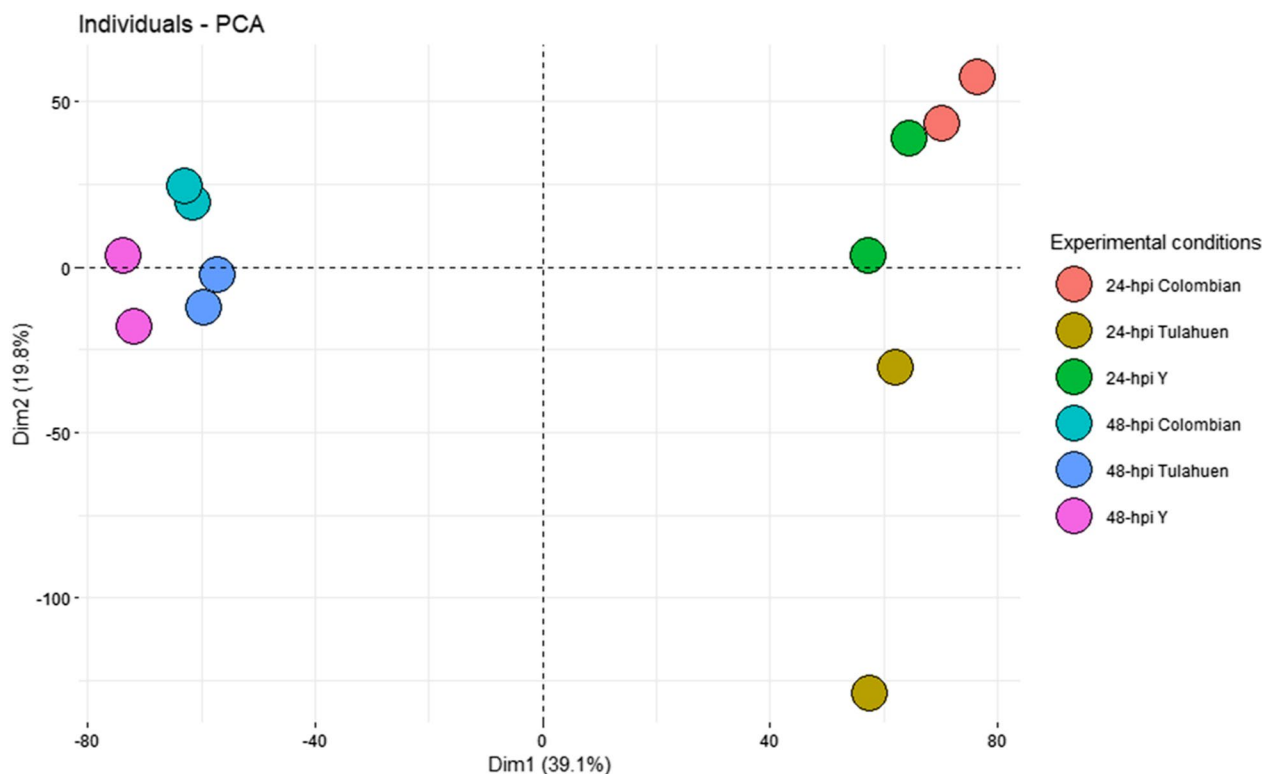


Fig. 5 Principal component analysis plot of the transcriptional profile of the in vitro cardiomyocyte infection models. Principal component analysis plot, based on the fold-change (vs control) values of the 10,784 valid genes. Each dot represents a biological condition at 24- or 48-h post-infection. The principal components 1 and 2 together describe 58.9% of the total variance in the dataset. *Dim* dimension

A biased search of inflammation-related genes returned five cytokines and chemokines that were differentially expressed among all three cardiomyocyte infection conditions, namely *Gdf-15*, *Cxcl10*, *Cxcl2*, *Il-6* and *Tnf*. The expression levels of these inflammatory cytokines were significantly higher in the three cardiomyocyte infection conditions compared to the non-infected control: Colombian strain $P=0.0024$, Y strain $P=0.001$ and Tulahuen strain $P=0.0014$ (Fig. 8).

Transcriptomic remodeling unique to Colombian- and Y-infections

Upregulated genes over-represented the DEGs shared among the Colombian- and Y-infected conditions and thus formed the focus of our interest. Such 331 genes enriched pathways related to 'DNA replication ($Z=6.8$, $P<0.001$)', 'One Carbon metabolism ($Z=6.8$, $P<0.001$)', 'Nucleotide metabolism ($Z=6.8$, $P<0.001$)', 'Glutathione and one-carbon metabolism ($Z=5.1$, $P<0.01$)', and 'Mitochondrial gene expression ($Z=4.9$, $P<0.01$)' (Fig. 9A). The same gene list was enriched in genes associated with the Biological Process GO terms of 'Nucleic acid metabolic process' ($Z=8.3$, $P<0.001$), 'Nucleobase-containing

compound metabolic process ($Z=7.2$, $P<0.001$), 'Heterocycle metabolic process' ($Z=7.1$, $P<0.001$), 'Cellular nitrogen compound metabolic process' ($Z=6.9$, $P<0.001$), 'Cellular aromatic compound metabolic process' ($Z=6.9$, $P<0.001$), 'Organic cyclic compound metabolic process' ($Z=6.8$, $P<0.001$), 'Nitrogen compound metabolic process' ($Z=6.7$, $P<0.001$), 'RNA metabolic process' ($Z=6.9$, $P<0.001$), and 'Gene expression' ($Z=6.1$, $P<0.001$) (Fig. 9B).

Differentially expressed genes corresponding to the 'Glutathione and one-carbon metabolism' pathway (Wikipathway ID: WP730) were individually tracked and analyzed, where the genes corresponding to the 'one-carbon metabolism' and 'Glutathione metabolism' showed an up and downregulation trend, respectively. Shared, as well as Colombian/Y-unique, pathways and GO terms enriched with upregulated DEGs upon infection are summarized in Table 1.

Transcriptomic remodeling unique to Tulahuen-infections

Tulahuen-infection led to the unique downregulation of 218 DEGs in the cardiomyocyte transcriptome. Significantly enriched pathways were: 'Proteasome degradation' ($Z=5.1$, $P<0.001$), 'Electron transport chain'

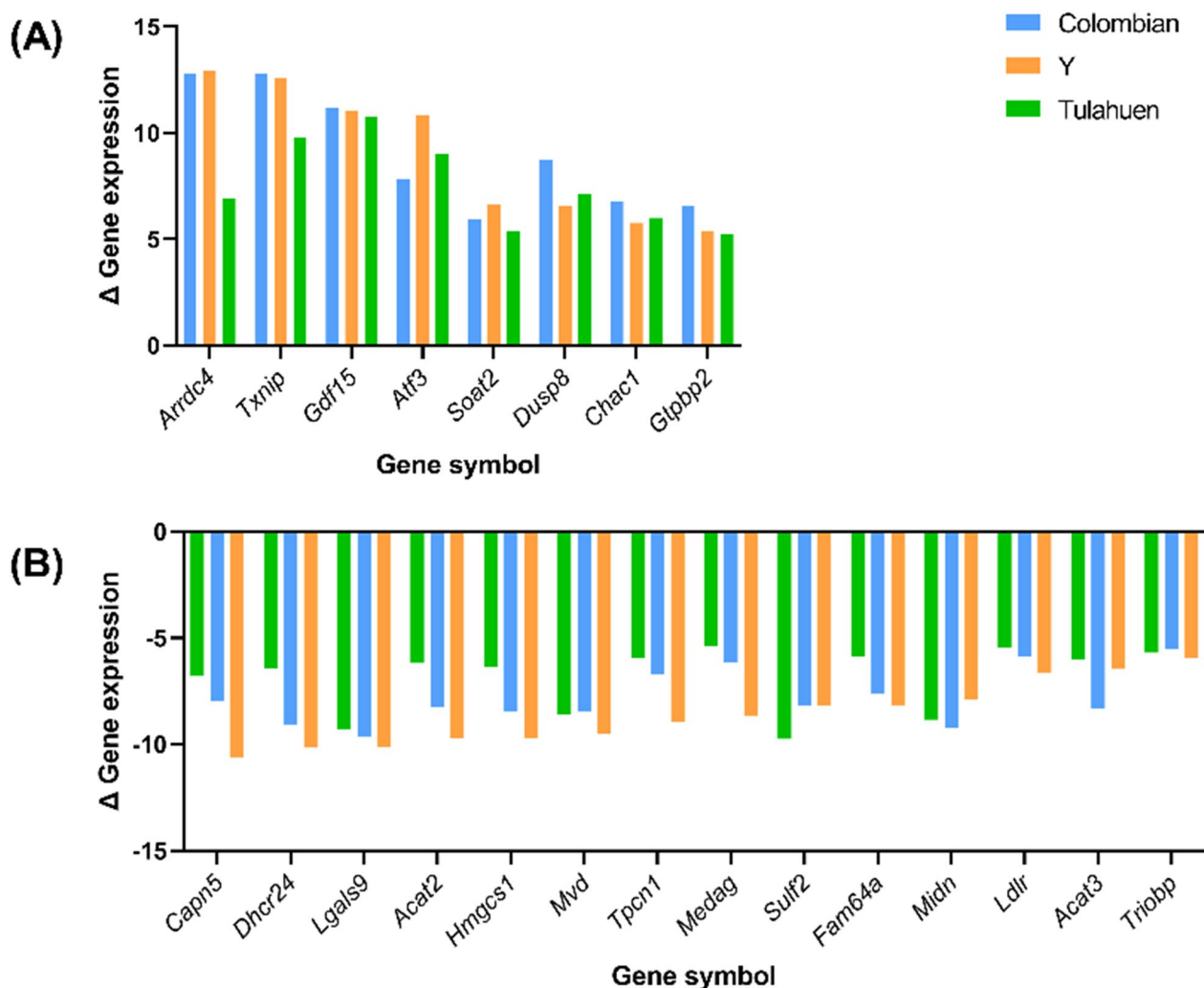


Fig. 6 Top differentially expressed genes of the cardiomyocyte upon *Trypanosoma cruzi* infection. Extensively **A** upregulated (fold-change > 5) and **B** downregulated (fold-change < 0.2) genes of the cardiomyocyte at 24-h post-infection are listed. Δ Gene expression, the fold-change or ratio between gene expression level of the infected cardiomyocytes and the non-infected negative control. *Aradc4* arrestin domain containing 4, *Txnip* thioredoxin interacting protein, *Gdf15* growth differentiation factor 15, *Atf3* activating transcription factor 3, *Soat2* sterol α -acyltransferase 2, *Dusp8* dual specificity phosphatase 8, *Chac1* cation transport regulator 1, *Gtbbp2* GTP binding protein 2, *Capn5* Calpain 5, *Dhcr24* 24-dehydrocholesterol reductase, *Lgals9* lectin galactose binding soluble 9, *Acat2* acetyl-coenzyme A acetyltransferase 2, *Hmgcs1* 3-hydroxy-3-methylglutaryl-Coenzyme A synthase 1, *Mvd* mevalonate (diphospho) decarboxylase, *Tpcn1* two pore channel 1, *Medag* mesenteric estrogen dependent adipogenesis, *Sulf2* sulfatase 2, *Fam64a* family with sequence similarity 64 member A, *Midn* midnolin, *Ldlr* low density lipoprotein receptor, *Acat3* acetyl-coenzyme A acetyltransferase 3, *Triobb* TRIO and F-actin binding protein

($Z=4.1$, $P<0.01$), and ‘Oxidative phosphorylation’ ($Z=3.7$, $P<0.01$). Top 10 Biological processes GO terms enriched by this gene set are ‘Cellular metabolic process’ ($Z=3.9$, $P<0.001$), ‘Metabolic process’ ($Z=3.4$, $P<0.001$), ‘Cellular process’ ($Z=2.3$, $P<0.001$), ‘Organic substance metabolic process’ ($Z=3.2$, $P<0.001$), ‘Localization’ ($Z=4.0$, $P<0.001$), ‘Organic substance transport’ ($Z=4.5$, $P<0.001$), ‘Macromolecule localization’ ($Z=4.4$, $P<0.001$), ‘Cellular protein metabolic process’ ($Z=3.9$, $P<0.001$), and ‘Cellular protein metabolic process’ ($Z=3.9$, $P<0.001$).

Trypanosoma cruzi infection increases intracellular reactive oxygen species in HL-1 cardiomyocytes

With specific interest in the accentuated ROS mitigation response elucidated from transcriptomic analysis of the cellular models, we next evaluated the intracellular ROS level of infected cardiomyocytes. HL-1 cardiomyocytes showed higher ROS levels upon infection with *T. cruzi* in comparison to non-infected controls. Signal intensity (mean, interquartile range) of the ROS-specific fluorescent dye, CellRox green, was significantly higher in the *T. cruzi*-infected condition (16.55,

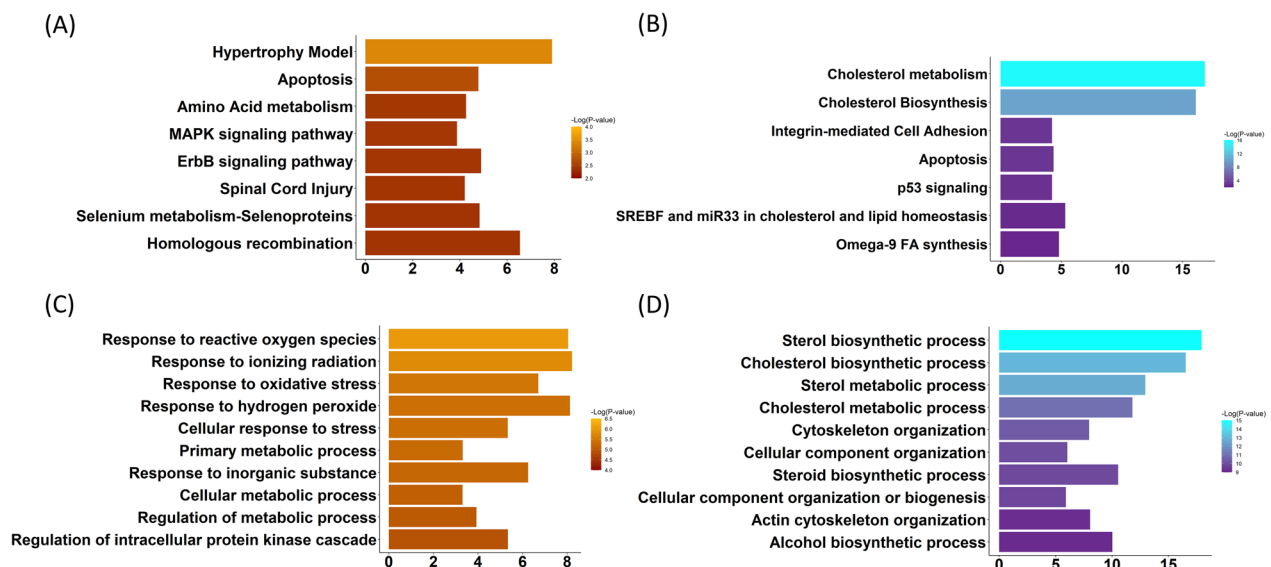


Fig. 7 Signatures of the common cardiomyocyte response to *Trypanosoma cruzi* infection. **A, B** 'WikiPathways' and **C, D** 'Biological Process gene ontology Terms' enriched by commonly **A, C** upregulated and **B, D** downregulated genes of the host cardiomyocyte at 24-h post-infection are sorted based on *P*-value. Bar lengths represent enrichment Z-scores

9.73–19.02; 6.85, 5.70–7.54; $P < 0.0001$), further validating the relevant role of ROS in CCM pathogenesis (Fig. 10A). Representative images are shown in Fig. 10B.

Discussion

In vitro infection using HL-1 cardiomyocytes and *T. cruzi* from different genetic strains provided mechanistic clues to CCM progression.

Subsequent transcriptomic and functional analyses of the in vitro cardiomyocyte infection models had characterized in-depth the myocardial innate response that is a potential determinant of CCM progression. The cross-strain comparative analysis led to the characterization of the universal hallmarks of the cardiomyocyte response against *T. cruzi* infection, consisting of DEGs evoked under all three infection conditions. Among the hallmark transcriptomic signatures were pathways related to oxidative stress (the 'Response to reactive oxygen species', 'Response to oxidative stress', 'Response to hydrogen peroxide' GO terms), cell proliferation and cardiac hypertrophy (the 'ErbB signaling', 'Hypertrophy model' and 'MAPK signaling' pathways), and those related to heart energy metabolism (the 'SREBF and miR33 in cholesterol and lipid homeostasis', and 'Omega-9 FA synthesis' pathways and the 'Sterol biosynthetic process', 'Cholesterol biosynthetic process', 'Sterol metabolic process', 'Cholesterol metabolic process' and 'Steroid biosynthetic process' GO terms).

Firstly, possible derangements in cardiomyocyte ROS homeostasis, as observed here in our cellular model, has been previously reported to accompany cardiac infection with *T. cruzi* [27, 29, 31, 38–40]. ROS mitigation is not a unique host response but in fact a shared mechanism of the cardiomyocyte against the more common insults leading to dilated cardiomyopathy, namely ischemia/hypoxia and Coxsackie virus infection [41–43]. Among the unique remodeling patterns in Colombian and Y infections were the upregulation of glutathione metabolism for ROS mitigation in CCM progression. Previous in vitro [23, 24] and in vivo studies [22] have shown that glutathione and its related metabolites serve as key antioxidants in cardiomyocytes under infectious or hypoxic stress [44–46]. Altogether, the concomitant upregulation of the compensatory 'Glutathione and one-carbon metabolism' pathways in Colombian- and Y-infected cardiomyocytes further highlights the intriguing role of ROS homeostasis in CCM pathogenesis. Several genes from the 'Hypoxia signaling' pathway, notably the hypoxia-inducible factor 1- α (HIF-1 α) have been reported to be upregulated in human cardiomyocytes as a response to infection with *T. cruzi* [18]. HIF-1 α has been reported to be positively correlated with myocarditis severity in patients with CCM [47]. Although in our dataset the 'hypoxia signaling' pathway was not enriched, a detailed search of HIF-1 α -targeted genes revealed the downregulation of *Glutathione peroxidase 3 (Gpx3)*, and the upregulation of *Growth Arrest and DNA Damage Inducible*

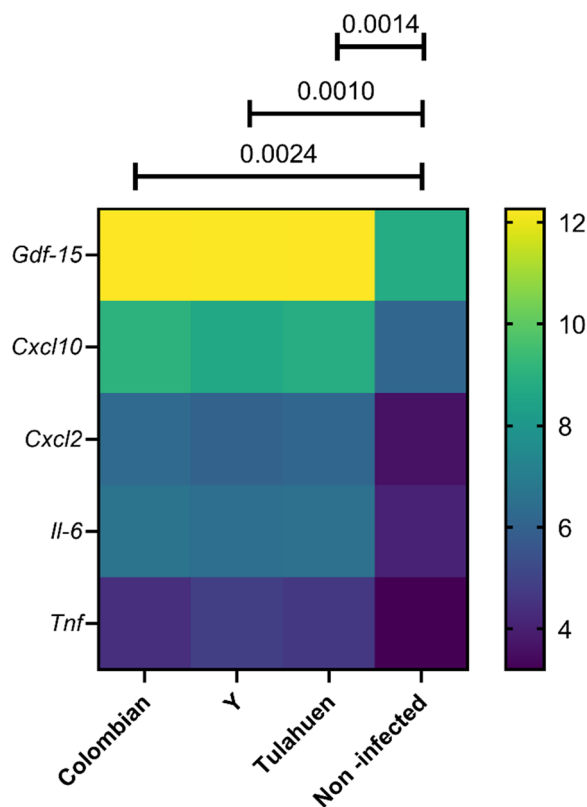


Fig. 8 Heatmap of expression levels of inflammation-related genes in HL-1 cells infected with *T. cruzi* at 24-h post-infection. Genes are represented in rows and infection conditions are represented in columns. Color legend represents the logarithm 2 of gene expression level. *P*-values were calculated by paired T-test. *Gdf-15* growth differentiation factor 15, *Cxcl10* C-X-C motif chemokine ligand 10, *Cxcl2* C-X-C motif chemokine ligand 2, *Il-6* interleukin-6, *Tnf* tumor necrosis factor-alpha

Alpha (Gadd45a). An overtime decline of glutathione peroxidase levels has been previously described in a CCM model after an initial burst on its levels triggered by chronic ROS accumulation typical of hypoxic states [48], and might promote progression to heart failure [49].

Secondly, upregulation of cell proliferation pathways, such as 'PI3K/AKT', 'Extracellular signal-regulated kinases 1 and 2 (ERK1/2)', 'JAK/STAT signaling' and 'The mammalian target of Rifampicin (mTORC)' pathways, have been shown previously in multiple studies with human and murine cell lines infected with a variety of *T. cruzi* strains [24, 29, 50–59]. Cell proliferation seems a shared response mechanism among variable host cells, considering the differential expression of 18 well-known pro-proliferative genes, including *Rhob*, *Atf3*, *Brca2*, *Jun*, *Jund*, *Myc*, as well as the enrichment in the mutually interacting pathways of ErbB and MAPK

signaling, observed in the cardiomyocyte response of our data set [56]. A summarization of the DEGs of the ErbB and MAPK signaling pathways is depicted in Additional file 2: Fig. S3. In the context of cardiomyocytic responses, although initially adaptive to stress stimuli, such signaling pathways are the underlying cause of pathological cardiac hypertrophy and mechanical dysfunction when chronically activated [60–62]. Thus, these pathways have constituted the 'double-edged' roles in the development of, and the common potential targets for, ischemic and viral cardiomyopathies [63–65].

Thirdly, cellular metabolism can drastically influence cellular functions in the failing heart [66, 67]. Previous in vitro studies have replicated downregulation of key genes in lipid metabolism such as *Dhcr24* [23, 68]. The uncoupling of heart lipid synthesis and β -oxidation, coined cardiac lipidopathy, has been suggested as a hallmark metabolic feature of CCM [69]. Sterol regulatory element binding factor (*Srebf*), a transcription factor that regulates cellular lipid homeostasis by controlling the expression of an array of enzymes required for endogenous cholesterol, fatty acid, triacylglycerol, and phospholipid synthesis [70, 71] was found to be one of the commonly downregulated DEGs in our dataset at 24 and 48 hpi (Additional file 1). *Srebf* has been proposed as a potential target for ameliorating the cardiac lipidopathy in Chagas disease [72, 73]. This imbalance of lipid synthesis and beta-oxidation became further prominent in our in vitro model at 48 hpi, accompanied by the downregulation of 'Fatty acid oxidation' and 'Beta-oxidation' pathway-related genes: *Acss2*, *Acsl4*, and *Acsl5* (Additional file 1). The correction of such pathogenic metabolic uncoupling that may potentiate *T. cruzi* proliferation may exert therapeutic potential against CCM through the restoration of metabolic homeostasis [73–75]. While the glycolysis pathway was not significantly enriched in our dataset, a manual search of glucose metabolism-related genes showed the common upregulation of *Solute Carrier Family 2 Member 3*. The upregulation of *6-phosphofructo-2-kinase/fructose-2,6-biphosphatase 3* and *Phosphoglycerate mutase family member 5* in Colombian and Y-infected cells only; and the downregulation of *Solute Carrier Family 2 Member 1* and *Phosphofructokinase, liver, B-type* in Tulahuen infection. Noteworthy, *Arrestin Domain Containing 4 (Arrdc4)*, *Thioredoxin interacting protein (Txnip)*, and *Activating transcription factor 3 (Atf3)*, which were among the most extensively upregulated genes common to all cardiomyocyte infection conditions, may hinder glucose uptake and lead to apoptosis in vitro as shown in murine cardiomyocytes and *T. cruzi*-infected human fibroblasts [76–80]. Their upregulation

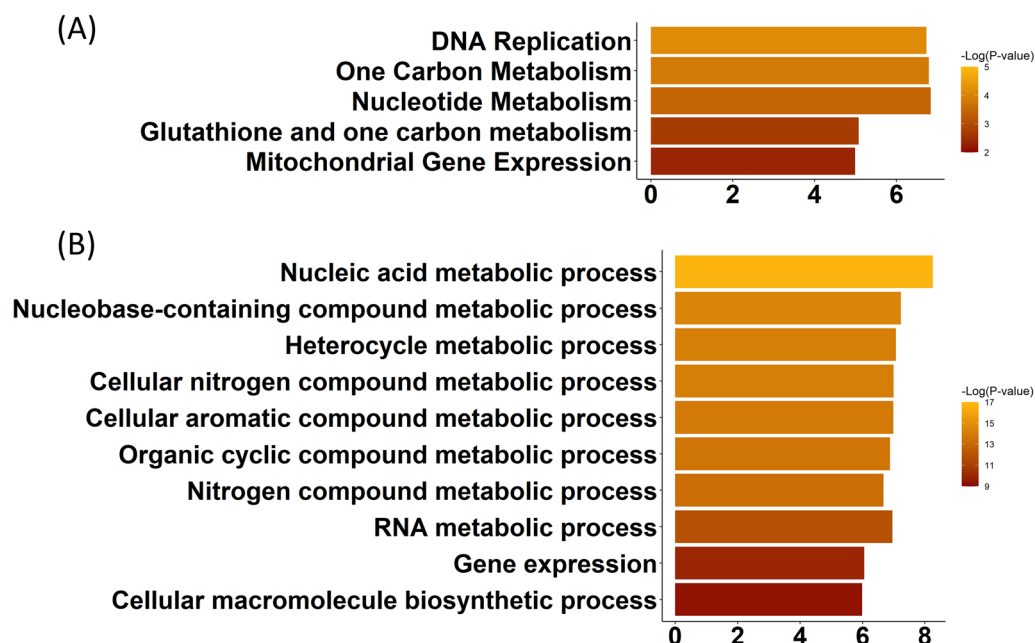


Fig. 9 Signatures of transcriptomic remodeling unique to Colombian- and Y-infections. 'WikiPathways' (A) and 'Biological Process gene ontology Terms' (B), enriched by the genes uniquely upregulated at 24-h post-infection in Colombian- and Y-infected cardiomyocytes are sorted based on *P*-value. Bar lengths represent enrichment Z-scores

in vivo promotes cardiac hypertrophy and contractile dysfunction [81, 82]. Furthermore, *Atf3*, which is induced by ROS and pathogens including *T. cruzi*, may promote fibrosis and cardiac hypertrophy [83–89]. *T. cruzi*-infected Induced Pluripotent Stem Cardiomyocytes (iPS-CM) display an activation of the glycolysis and oxidative phosphorylation pathway where attenuation of glucose uptake significantly decreased parasites' invasion and replication within the host [18]. The aforementioned phenomenon has also been observed after restricting the cell from other carbon sources like glutamine [90]. This number of phenotypic effects derived from their dysregulation renders them an interesting group of genes to explore their role in the pathogenesis of CCM. Further functional analysis in vitro on actual glucose utilization using our cellular model may elucidate whether a metabolic compensatory mechanism is operating to mitigate the ongoing infection.

Additionally, among the top upregulated DEGs was the TGF- β superfamily *Gdf15*, an emerging cardiovascular biomarker. GDF15 protects cardiomyocytes from ROS- and nitric oxide-induced apoptosis in vitro. In addition, the risk stratification potential of GDF15 in patients with heart failure is currently gaining attention [91–93]. Given that the upregulation of GDF15 comprises the cardinal feature of cardiomyocyte response in our in vitro model, the behavior of this cytokine in actual CCM patients arises as our next intriguing research question.

Regional factors, including circulating *T. cruzi* strains, have attracted attention as likely determinants of Chagas disease phenotypic expression and CCM progression [94–99]. Experimental data from murine and cellular models of CCM have shown that *T. cruzi* Colombian and Y strains among others cause severe myocarditis and higher mortality [22, 100, 101]. Epidemiological data from Colombian, Brazilian and Argentinian patients suggest that CCM prevalence and severity is increased in those infected with certain *T. cruzi* strains [102–105]. Although not the only causative factor, it is likely that infections caused by parasites of specific genetic traits render the host prone to severe CCM forms.

The limitations of this study include the lack of normalization of the gene expression values by intracellular amastigote burden across the infecting *T. cruzi* strains. Higher infectivity was observed in the Colombian and Y strains compared with the Tulahuen strain and may have affected the time course of progression of the in vitro pathogenesis. Such a trend towards less infectivity of the Tulahuen strain has been observed in previous studies [106, 107]. Single-cell resolution analyses, to overcome the weaknesses of bulk transcriptomics, may aid in eliminating potential interpretation biases of the observed inter-strain differences from the current approach. It is also noteworthy that since the present study was mainly observational in nature, further functional experiments are to be performed in order to make conclusions about

Table 1 Summarization of the pathways enriched by the upregulated genes in all the *T. cruzi*-infection conditions

	Pathway name	Common	Exclusive to Colombian/Y strain	
Upregulated WikiPathways	DNA replication		○	
	One carbon metabolism		○	
	Glutathione and one-carbon metabolism		○	
	Nucleotide metabolism		○	
	Mitochondrial gene expression		○	
	Hypertrophy model	○		
	Homologous recombination	○		
	Apoptosis	○		
	ErbB signaling pathway	○		
	Selenium metabolism selenoproteins	○		
	Amino acid metabolism	○		
	Spinal cord injury	○		
	MAPK signaling pathway	○		
	Upregulated biological process GO terms	Nucleic acid metabolic process		○
		Nucleobase-containing compound metabolic process		○
Heterocycle metabolic process			○	
Cellular nitrogen compound metabolic process			○	
Cellular aromatic compound metabolic process			○	
Organic cyclic compound metabolic process			○	
Nitrogen compound metabolic process			○	
RNA metabolic process			○	
Gene expression			○	
Response to reactive oxygen species		○		
Response to ionizing radiation		○		
Response to oxidative stress		○		
Response to hydrogen peroxide		○		
Cellular response to stress		○		
Primary metabolic process		○		
Response to inorganic substance		○		
Regulation of metabolic process		○		
Regulation of intracellular protein kinase cascade	○			

the relevance of the individual pathways that were highlighted here.

Conclusions

In conclusion, the ubiquitously observed hypertrophic and oxidative stress-related transcriptome remodeling are universal hallmarks of the cardiomyocyte response

against *T. cruzi* infection. The Colombian and Y strain elicited an accentuated response in cardiomyocyte ROS mitigation, nitrogen, and glutathione metabolism suggesting a role in CCM progression. The downregulation of the cardiomyocyte's energy metabolic pathways exclusively observed in the Tulahuen strain infection may enact a protective effect against the infection.

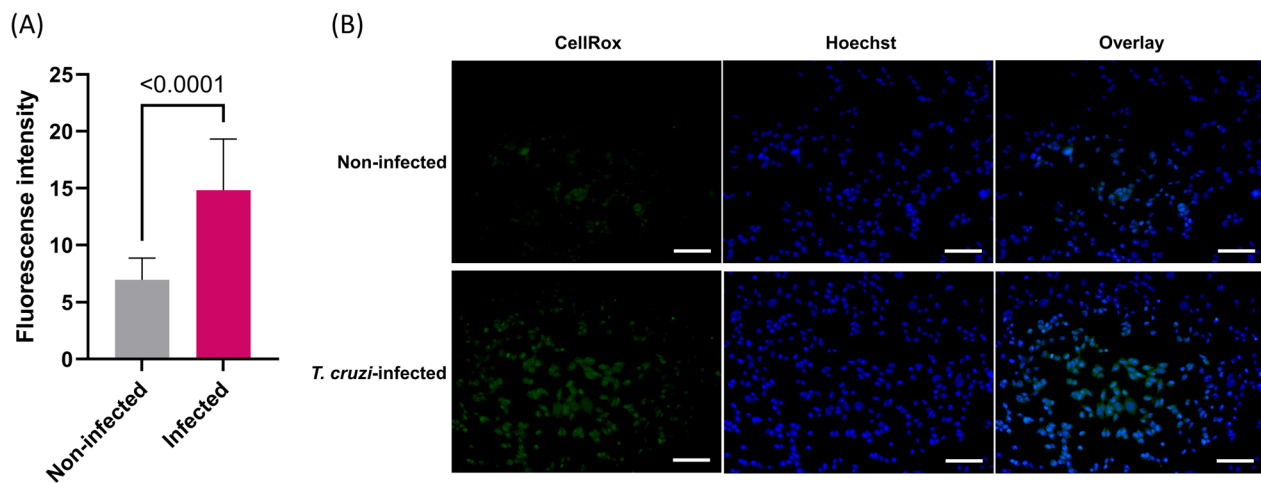


Fig. 10 Elevated intracellular levels of reactive oxygen species in *Trypanosoma cruzi*-infected cardiomyocytes. **A** Signal intensity of reactive oxygen species-specific fluorescence was higher in the cardiomyocytes infected with the Y strain at 24-h post-infection, compared with non-infected control cells. Statistical comparison was performed with Mann–Whitney test. Bars represent mean fluorescence intensity and error bars represent standard deviation. **B** Representative fluorescence microscopy images from reactive oxygen species-specific CellRox green staining. Comparison with the non-infected (upper) control cells shows higher intensity of reactive oxygen species fluorescence signal in the cardiomyocytes 24-h post-infection with *Trypanosoma cruzi* Y strain (lower). Scale bars represent 100 μ m

Abbreviations

<i>Arddc4</i>	Arresting domain containing 4
<i>Atf3</i>	Activating transcription factor 3
CCdT	Cultured cell-derived trypomastigotes
CCM	Chagas cardiomyopathy
DAS	Data availability statement
DEG	Differentially expressed genes
FC	Fold change
<i>Gdf15</i>	Growth/differentiation factor 15
GO	Gene ontology
hpi	Hours post-infection
LIT	Liver infusion tryptose
MOI	Multiplicity of infection
<i>P</i>	<i>P</i> -Value
PBS	Phosphate buffered saline
PCA	Principal component analysis
ROS	Reactive oxygen species
<i>T. cruzi</i>	<i>Trypanosoma cruzi</i>
<i>Tnf</i>	Tumor necrosis factor
TNF- α	Tumor necrosis factor α
<i>Txnip</i>	Thioredoxin interacting protein
Z	Z-score

Supplementary Information

The online version contains supplementary material available at <https://doi.org/10.1186/s41182-023-00552-6>.

Additional file 1: Valid gene set at 24 and 48 hpi. Valid gene probes above the thresholds of intensity in every infection condition at 24- and 48-hpi timepoints.

Additional file 2: Figure S1. Representative images of *Trypanosoma cruzi*-infected cardiomyocytes reflecting infectivity rate differences among strains. Diff-Quick staining. Scale bars represent 50 μ m. **Figure S2.** Remodeling of gene expression profiles in cardiomyocytes treated with Tumor Necrosis Factor- α (Positive control) at 24- and 48-h post-infection (hpi). Y axes indicate the gene expression level of the non-infected control cardiomyocyte, while X-axes indicate gene expression levels of Tumor Necrosis Factor-treated cardiomyocytes. The black dashed line, and upper

and lower red dashed lines show the line of identity, and the 0.5- and 2-fold-change thresholds, respectively. Each dot represents a differentially expressed gene (DEG). Blue and pink shaded areas represent down- and up-regulated DEGs, respectively. **Figure S3.** Cytoscape network visualization of the *Mus musculus* 'Erbb-' and 'MAPK signaling' pathways. Network showing the commonly upregulated genes of both pathways (orange nodes) and their two closest neighbors (light blue nodes). Red and purple circles enclose genes that belong to the 'Erbb-' and 'MAPK signaling' pathways, respectively. Edges (black lines) represent links between genes.

Acknowledgements

We would like to especially thank Mrs. Mika Oku and Mrs. Mika Shinohara for their technical assistance in performing the experimental procedure. We also appreciate the valuable comments on the manuscript given by the researchers from the Virology and Parasitology department.

Author contributions

KSCM, and YN conceptualized and designed the study, performed the experiments, and wrote the manuscript. MI validated the methods. KSCM, YN, SN, and ETK conducted data analysis and graph generation. NT, YS, YNi, YMN, NK, YO, CEA, MM, KA, SP, YMa, IK, and JNS critically appraised the manuscript and interpreted the results of the analyses. YK substantially revised the manuscript. All authors have reviewed the manuscript drafts and approved the final version.

Funding

This research was supported by Grants from the Japan Agency for Medical Research and Development (AMED) (JP21wm0325049 to Yu Nakagama, and JP21jm0110016 to Junko Nakajima-Shimada and Yasutoshi Kido), the Japan Society for the Promotion of Science (19K23992 to Yu Nakagama), and 16H06279 to the Platform for Advanced Genome Science (PAGS) and the Ohyama Health Foundation (to Yu Nakagama). This work was performed as part of the Science and Technology Research Partnership for Sustainable Development (SATREPS) program co-organized by the AMED and the Japan International Cooperation Agency (JICA).

Availability of data and materials

The data that support the findings of this study are openly available in Mendeley Data, at <http://doi.org/10.17632/v82vdk7ws.2>

Declarations

Ethics approval and consent to participate

Our research use of animal cells adheres to the fundamental principles of the Basel Declaration and the International Council for Laboratory Animal Science (ICLAS) and complies with our institutional guidelines.

Consent for publication

Not applicable.

Competing interests

The authors declare that they have no competing interests.

Author details

¹Department of Parasitology, Graduate School of Medicine, Osaka Metropolitan University, 1-4-3 Asahi-machi, Abeno-ku, Osaka 545-8585, Japan. ²Research Center for Infectious Disease Sciences, Graduate School of Medicine, Osaka Metropolitan University, 1-4-3 Asahi-machi, Abeno-ku, Osaka 545-8585, Japan. ³Centro Nacional de Investigaciones Científicas de El Salvador (CICES), Ciudad Universitaria "Dr. Fabio Castillo Figueroa", final avenida "Mártires del 30 de julio", San Salvador, El Salvador. ⁴Department of Cardiovascular Medicine, Graduate School of Medicine, The University of Tokyo, 7-3-1 Hongo, Bunkyo-ku, Tokyo 113-0033, Japan. ⁵Department of Advanced Clinical Science and Therapeutics, Graduate School of Medicine, The University of Tokyo, 7-3-1 Hongo, Bunkyo-ku, Tokyo 113-0033, Japan. ⁶Department of Cardiovascular Medicine, Graduate School of Medical and Dental Sciences, Tokyo Medical and Dental University, 1-5-45 Yushima, Bunkyo-ku, Tokyo 113-8519, Japan. ⁷Department of Internal Medicine, University of Mbujimayi, #1 avenue de l'Université, Dibindi, 225, Mbujimayi, Democratic Republic of Congo. ⁸Division of Cardiology and Metabolism, Center for Molecular Medicine, Jichi Medical University, 3311-1 Yakushiji, Shimotsuke 329-0498, Japan. ⁹Center for Cancer Immunotherapy and Immunobiology, Kyoto University Graduate School of Medicine, Yoshida Nihonmatsucho, Sakyo-ku, Kyoto 606-8501, Japan. ¹⁰Department of Molecular and Cellular Parasitology, Graduate School of Health Sciences, Gunma University, 3-39-22 Showa-machi, Maebashi, Gunma 371-8514, Japan. ¹¹Departamento de Investigación, Hospital Nacional Especializado "Rosales", Ministerio de Salud de El Salvador, Calle Arce No. 827, San Salvador, El Salvador. ¹²International University of Health and Welfare, Minato-Ku, Tokyo 107-8402, Japan. ¹³Department of Frontier Cardiovascular Medicine, Graduate School of Medicine, The University of Tokyo, Bunkyo-ku, Tokyo 113-8655, Japan.

Received: 26 July 2023 Accepted: 22 October 2023

Published online: 07 December 2023

References

- Chagas C. Nova tripanozomíaze humana: estudos sobre a morfologia e o ciclo evolutivo do *Schizotrypanum cruzi* n. gen., n. sp., agente etiológico de nova entidade morbida do homem. Mem Inst Oswaldo Cruz. 1909;1(2):159–218.
- Chagas disease—PAHO/WHO|Pan American Health Organization. <https://www.paho.org/en/topics/chagas-disease>. Accessed 26 Dec 2022.
- Lidani KCF, Andrade FA, Bavia L, Damasceno FS, Beltrame MH, Messias-Reason IJ, et al. Chagas disease: from discovery to a worldwide health problem. Front Public Health. 2019;7:166.
- Nunes MCP, Beaton A, Acquatella H, Bern C, Bolger AF, Echeverría LE, et al. Chagas cardiomyopathy: an update of current clinical knowledge and management: a scientific statement from the American Heart Association. Circulation. 2018;138(12):e169-209. <https://doi.org/10.1161/CIR.0000000000000599>.
- Stride N, Larsen S, Hey-Mogensen M, Hansen CN, Prats C, Steinbrüchel D, et al. Impaired mitochondrial function in chronically ischemic human heart. Am J Physiol Heart Circ Physiol. 2013;304(11):1407–14.
- Knowlton KU. Dilated cardiomyopathy: viral persistence and a role for a viral proteinase in human hearts. Circulation. 2019;139(20):2339.
- Bouin A, Gretteau PA, Wehbe M, Renois F, N'Guyen Y, Lévêque N, et al. Enterovirus persistence in cardiac cells of patients with idiopathic dilated cardiomyopathy is linked to 5' terminal genomic RNA-deleted viral populations with viral-encoded proteinase activities. Circulation. 2019;139(20):2326–38. <https://doi.org/10.1161/CIRCULATIONAHA.118.035966>.
- Bayeva M, Teodor K. Molecular and cellular basis of viable dysfunctional myocardium. 2014. <http://circheartfailure.ahajournals.org>. Accessed 26 Dec 2022.
- Page BJ, Young RF, Suzuki G, Fallavollita JA, Canty JM. The physiological significance of a coronary stenosis differentially affects contractility and mitochondrial function in viable chronically dysfunctional myocardium. Basic Res Cardiol. 2013. <https://doi.org/10.1007/s00395-013-0354-0>.
- Hershberger RE, Pinto JR, Parks SB, Kushner JD, Li D, Ludwigsen S, et al. Clinical and functional characterization of TNNT2 mutations identified in patients with dilated cardiomyopathy. Circ Cardiovasc Genet. 2009;2(4):306–13. <https://doi.org/10.1161/CIRCGENETICS.108.846733>.
- Poller W, Fechner H, Noutsias M, Tschoepe C, Pauschinger M, Schultheiss HP. The molecular basis of cardiotropic viral infections. Eur Heart J Suppl. 2002;4(Suppl_1):18-30.
- Rao L, Debbas M, Sabbatini P, Hockenbery D, Korsmeyer S, White E. The adenovirus E1A proteins induce apoptosis, which is inhibited by the E1B 19-kDa and Bcl-2 proteins. Proc Natl Acad Sci USA. 1992;89(16):7742–6.
- Kawai C. From myocarditis to cardiomyopathy: mechanisms of inflammation and cell death. Circulation. 1999;99(8):1091–100. <https://doi.org/10.1161/01.cir.99.8.1091>.
- Gougeon ML, Montagnier L. Apoptosis in AIDS. Science. 1993;260:1269.
- Debiasi RL, Robinson BA, Leser JS, Brown RD, Long CS, Clarke P. Critical role for death-receptor mediated apoptotic signaling in viral myocarditis. J Card Fail. 2010;16(11):901.
- Nogueira PM, Ribeiro K, Silveira ACO, Campos JH, Martins-Filho OA, Bela SR, et al. Vesicles from different *Trypanosoma cruzi* strains trigger differential innate and chronic immune responses. J Extracell Vesicle. 2015. <https://doi.org/10.3402/jev.v4.28734>.
- Bustamante JM, Rivarola HW, Fernandez AR, Enders JE, Fretes R, Palma JA, et al. Indeterminate Chagas' disease: *Trypanosoma cruzi* strain and re-infection are factors involved in the progression of cardiopathy. Clin Sci. 2003;104(4):415–20.
- Venturini G, Alvim JM, Padilha K, Toepfer CN, Gorham JM, Wasson LK, et al. Cardiomyocyte infection by *Trypanosoma cruzi* promotes innate immune response and glycolysis activation. Front Cell Infect Microbiol. 2023;6(13):1098457.
- Pereira IR, Vilar-Pereira G, Silva AA, Moreira OC, Britto C, Diana E, et al. Tumor necrosis factor is a therapeutic target for immunological unbalance and cardiac abnormalities in chronic experimental Chagas' heart disease. Mediators Inflamm. 2014. <https://doi.org/10.1155/2014/798078>.
- Bozzi A, Sayed N, Matsa E, Sass G, Neofytou E, Clemons KV, et al. Using human induced pluripotent stem cell-derived cardiomyocytes as a model to study *Trypanosoma cruzi* infection. Stem Cell Rep. 2019;12(6):1232–41.
- Rodrigues DBR, Dos Reis MA, Romano A, Pereira SADL, Teixeira VDBA, Tostes Junior S, et al. In situ expression of regulatory cytokines by heart inflammatory cells in Chagas' disease patients with heart failure. Clin Dev Immunol. 2012;2012:1–7.
- de Castro TBR, Canesso MCC, Boroni M, Chame DF, de Souza DL, de Toledo NE, et al. Differential modulation of mouse heart gene expression by infection with two *Trypanosoma cruzi* strains: a transcriptome analysis. Front Genet. 2020;11:1031.
- Adesse D, Garzoni LR, Meirelles MDN, Iacobas DA, Iacobas S, Spray DC, et al. Transcriptomic signatures of alterations in a myoblast cell line infected with four distinct strains of *Trypanosoma cruzi*. Am J Trop Med Hyg. 2010;82(5):846–54.
- Nisimura LM, Coelho LL, de Melo TG, de Vieira PC, Victorino PH, Garzoni LR, et al. *Trypanosoma cruzi* promotes transcriptomic remodeling of the JAK/STAT signaling and cell cycle pathways in myoblasts. Front Cell Infect Microbiol. 2020;10:255.

25. Contreras VT, Salles JM, Thomas N, Morel CM, Goldenberg S. In vitro differentiation of *Trypanosoma cruzi* under chemically defined conditions. *Mol Biochem Parasitol*. 1985;16(3):315–27.
26. Pissetti CW, Correia D, de Oliveira RF, Llaguno MM, Balarin MAS, Silva-Grecco RL, et al. Genetic and functional role of TNF- α in the development *Trypanosoma cruzi* infection. *PLoS Negl Trop Dis*. 2011;5(3):976.
27. Muñoz-Fernández MA, Fernández MA, Fresno M. Synergism between tumor necrosis factor- α and interferon- γ on macrophage activation for the killing of intracellular *Trypanosoma cruzi* through a nitric oxide-dependent mechanism. *Eur J Immunol*. 1992;22(2):301–7. <https://doi.org/10.1002/eji.1830220203>.
28. Chen Y, Pat B, Zheng J, Cain L, Powell P, Shi K, et al. Tumor necrosis factor- α produced in cardiomyocytes mediates a predominant myocardial inflammatory response to stretch in early volume overload. *J Mol Cell Cardiol*. 2010;49(1):70.
29. Cerbán FM, Stempin CC, Volpini X, Carrera Silva EA, Gea S, Motran CC. Signaling pathways that regulate *Trypanosoma cruzi* infection and immune response. *Biochim Biophys Acta BBA Mol Basis Dis*. 2020;1866(5):165707.
30. Krown KA, Page MT, Nguyen C, Zechner D, Gutierrez V, Comstock KL, et al. Tumor necrosis factor alpha-induced apoptosis in cardiac myocytes involvement of the sphingolipid signaling cascade in cardiac cell death. *J Clin Invest*. 1996;98:2854–65.
31. Silva JS, Vespa GNR, Cardoso MAG, Aliberti JCS, Cunha FQ. Tumor necrosis factor alpha mediates resistance to *Trypanosoma cruzi* infection in mice by inducing nitric oxide production in infected gamma interferon-activated macrophages. *Infect Immun*. 1995;63(12):4862.
32. R core Team. R: A language and environment for statistical computing. Vienna, Austria. 2022. <https://www.r-project.org/>. Accessed 26 Dec 2022.
33. Lê S, Josse J, Husson F. FactoMineR: an R package for multivariate analysis. *J Stat Softw*. 2008;25(1):1–18.
34. Kassambara A, Mundt F. factoextra: extract and visualize the results of multivariate data analyses. 2020. <https://cran.r-project.org/package=factoextra>. Accessed 26 Dec 2022
35. Martens M, Ammar A, Riutta A, Waagmeester A, Slenker DN, Hanspers K, et al. WikiPathways: connecting communities. *Nucleic Acids Res*. 2021;49(D1):D613–21.
36. Walter W, Sánchez-Cabo F, Ricote M. GOplot: an R package for visually combining expression data with functional analysis. *Bioinformatics*. 2015;31(17):2912–4.
37. Schneider CA, Rasband WS, Eliceiri KW. NIH Image to ImageJ: 25 years of image analysis. *Nat Methods*. 2012;9(7):671–5.
38. Dias PP, Capila RF, do Couto NF, Estrada D, Gadelha FR, Radi R, et al. Cardiomyocyte oxidants production may signal to *T. cruzi* intracellular development. *PLoS Negl Trop Dis*. 2017;11(8):e0005852. <https://doi.org/10.1371/journal.pntd.0005852>.
39. Machado FS, Martins GA, Aliberti JCS, Mestriner FLAC, Cunha FQ, Silva JS. *Trypanosoma cruzi*-infected cardiomyocytes produce chemokines and cytokines that trigger potent nitric oxide-dependent trypanocidal activity. *Circulation*. 2000;102(24):3003–8.
40. Gupta S, Bhatia V, Wen J-J, Wu Y, Huang MH, Garg NJ. *Trypanosoma cruzi* infection disturbs mitochondrial membrane potential and ROS production rate in cardiomyocytes. *Free Radic Biol Med*. 2009;47(10):1414–21.
41. Machado FS, Tanowitz HB, Ribeiro AL. Pathogenesis of Chagas cardiomyopathy: role of inflammation and oxidative stress. *J Am Heart Assoc*. 2013. <https://doi.org/10.1161/JAHA.113.000539>.
42. Tschöpe C, Ammirati E, Bozkurt B, Caforio ALP, Cooper LT, Felix SB, et al. Myocarditis and inflammatory cardiomyopathy: current evidence and future directions. *Nat Rev Cardiol*. 2020;18(3):169–93.
43. Tsutsui H, Kinugawa S, Matsushima S. Oxidative stress and heart failure. *Am J Physiol Heart Circ Physiol*. 2011;301(6):2181–90. <https://doi.org/10.1152/ajpheart.00554.2011>.
44. Pérez-Fuentes R, Guégan JF, Barnabé C, López-Colombo A, Salgado-Rosas H, Torres-Rasgado E, et al. Severity of chronic Chagas disease is associated with cytokine/antioxidant imbalance in chronically infected individuals. *Int J Parasitol*. 2003;33(3):293–9.
45. Wen J-J, Yachelini PC, Sembaj A, Manzur RE, Garg NJ. Increased oxidative stress is correlated with mitochondrial dysfunction in Chagasic patients. *Free Radic Biol Med*. 2006;41(2):270–6.
46. de Oliveira TB, Pedrosa RC, Filho DW. Oxidative stress in chronic cardiomyopathy associated with Chagas disease. *Int J Cardiol*. 2007;116(3):357–63.
47. Eberhardt N, Sanmarco LM, Bergero G, Favalaro RR, Vigliano C, Aoki MP. HIF-1 α and CD73 expression in cardiac leukocytes correlates with the severity of myocarditis in end-stage Chagas disease patients. *J Leukoc Biol*. 2021;109(1):233–44.
48. Wen JJ, Vyatkina G, Garg N. Oxidative damage during chagasic cardiomyopathy development: role of mitochondrial oxidant release and inefficient antioxidant defense. *Free Radic Biol Med*. 2004;37(11):1821–33.
49. Pang P, Abbott M, Abdi M, Fucci QA, Chauhan N, Mistri M, et al. Pre-clinical model of severe glutathione peroxidase-3 deficiency and chronic kidney disease results in coronary artery thrombosis and depressed left ventricular function. *Nephrol Dial Transplant*. 2018;33(6):923.
50. Libisch MG, Faral-Tello P, Garg NJ, Radi R, Piacenza L, Robello C. Early *Trypanosoma cruzi* infection triggers mTORC1-mediated respiration increase and mitochondrial biogenesis in human primary cardiomyocytes. *Front Microbiol*. 2018;9(Aug):397511.
51. Caradonna KL, Engel JC, Jacobi D, Lee CH, Burleigh BA. Host metabolism regulates intracellular growth of *Trypanosoma cruzi*. *Cell Host Microbe*. 2013;13(1):108–17.
52. Mukherjee S, Huang H, Petkova SB, Albanese C, Pestell RG, Braunstein VL, et al. *Trypanosoma cruzi* infection activates extracellular signal-regulated kinase in cultured endothelial and smooth muscle cells. *Infect Immun*. 2004;72(9):5274.
53. Hu X, Li J, Fu M, Zhao X, Wang W. The JAK/STAT signaling pathway: from bench to clinic. *Signal Transduct Target Ther*. 2021;6(1):1–33.
54. Márquez JDR, Ana Y, Baigorri RE, Stempi CC, Cerban FM. Mammalian target of rapamycin inhibition in *Trypanosoma cruzi*-infected macrophages leads to an intracellular profile that is detrimental for infection. *Front Immunol*. 2018;9(Feb):315838.
55. Libisch MG, Rego N, Robello C. Transcriptional studies on *Trypanosoma cruzi*—host cell interactions: a complex puzzle of variables. *Front Cell Infect Microbiol*. 2021. <https://doi.org/10.3389/fcimb.2021.692134>.
56. Wilkowsky SE, Barbieri MA, Stahl P, Isola ELD. *Trypanosoma cruzi*: phosphatidylinositol 3-kinase and protein kinase B activation is associated with parasite invasion. *Exp Cell Res*. 2001;264(2):211–8.
57. Chiribao ML, Libisch G, Parodi-Talice A, Robello C. Early *Trypanosoma cruzi* infection reprograms human epithelial cells. *Biomed Res Int*. 2014;2014:1–12.
58. Todorov AG, Einicker-Lamas M, De Castro SL, Oliveira MM, Guilherme A. Activation of host cell phosphatidylinositol 3-kinases by *Trypanosoma cruzi* infection. *J Biol Chem*. 2000;275(41):32182–6.
59. Silva MC, Davoli-Ferreira M, Medina TS, Sesti-Costa R, Silva GK, Lopes CD, et al. Canonical PI3Ky signaling in myeloid cells restricts *Trypanosoma cruzi* infection and dampens Chagasic myocarditis. *Nat Commun*. 2018;9(1):1–14.
60. Daneshgar N, Rabinovitch PS, Dai DF. TOR signaling pathway in cardiac aging and heart failure. *Biomolecules*. 2021;11(2):1–17.
61. Muslin AJ. MAPK signaling in cardiovascular health and disease: molecular mechanisms and therapeutic targets. *Clin Sci*. 2008;115(7):203.
62. Kishore R, Verma SK. Roles of STATs signaling in cardiovascular diseases. *JAKSTAT*. 2012;1(2):118.
63. Morellato AE, Umansky C, Pontel LB. The toxic side of one-carbon metabolism and epigenetics. *Redox Biol*. 2021;1:40.
64. Beck MA, Esworthy RS, Ho Y-S, Chu F-F. Glutathione peroxidase protects mice from viral-induced myocarditis. *FASEB J*. 1998;12(12):1143–9.
65. Koo S-J, Garg NJ. Metabolic programming of macrophage functions and pathogens control. *Redox Biol*. 2019;24:101198.
66. Taylor LA, Carthy CM, Yang D, Saad K, Wong D, Schreiner G, et al. Host gene regulation during coxsackievirus B3 infection in mice. *Circ Res*. 2000;87(4):328–34. <https://doi.org/10.1161/01.res.87.4.328>.
67. Abe H, Takeda N, Isagawa T, Semba H, Nishimura S, Suimye Morioka M, et al. Macrophage hypoxia signaling regulates cardiac fibrosis via Oncostatin M. *Nat Commun*. 2019. <https://doi.org/10.1038/s41467-019-10859-w>.

68. Imai K, Mimori T, Kawai M, Koga H. Microarray analysis of host gene-expression during intracellular nests formation of *Trypanosoma cruzi* amastigotes. *Microbiol Immunol*. 2005;49(7):623–31.
69. Teixeira PC, Ducret A, Langen H, Nogoceke E, Santos RHB, Silva Nunes JP, et al. Impairment of multiple mitochondrial energy metabolism pathways in the heart of Chagas disease cardiomyopathy patients. *Front Immunol*. 2021;12(12):755782.
70. Horton JD, Goldstein JL, Brown MS. SREBPs: activators of the complete program of cholesterol and fatty acid synthesis in the liver. *J Clin Invest*. 2002;109(9):1125–31.
71. Eberlé D, Hegarty B, Bossard P, Ferré P, Fougère F. SREBP transcription factors: master regulators of lipid homeostasis. *Biochimie*. 2004;86(11):839–48.
72. Ayyappan JP, Lizardo K, Wang S, Yurkow E, Nagajyothi JF. Inhibition of SREBP improves cardiac lipidopathy, improves endoplasmic reticulum stress, and modulates chronic Chagas cardiomyopathy. *J Am Heart Assoc*. 2020. <https://doi.org/10.1161/JAHA.119.014255>.
73. Johndrow C, Nelson R, Tanowitz H, Weiss LM, Nagajyothi F. *Trypanosoma cruzi* infection results in an increase in intracellular cholesterol. *Microbes Infect*. 2014;16(4):337–44.
74. Pereira MG, Nakayasu ES, Sant'Anna C, de Cicco NNT, Atella GC, de Souza W, et al. *Trypanosoma cruzi* epimastigotes are able to store and mobilize high amounts of cholesterol in reservosome lipid inclusions. *PLoS ONE*. 2011;6(7):e22359. <https://doi.org/10.1371/journal.pone.0022359>.
75. Pereira MG, Visbal G, Costa TFR, Frases S, de Souza W, Atella G, et al. *Trypanosoma cruzi* epimastigotes store cholesteryl esters in lipid droplets after cholesterol endocytosis. *Mol Biochem Parasitol*. 2018;1(224):6–16.
76. Patwari P, Chutkow WA, Cummings K, Verstraeten VLRM, Lammerding J, Schreiter ER, et al. Thioredoxin-independent regulation of metabolism by the alpha-arrestin proteins. *J Biol Chem*. 2009;284(37):24996–5003.
77. Kaimul AM, Nakamura H, Masutani H, Yodoi J. Thioredoxin and thioredoxin-binding protein-2 in cancer and metabolic syndrome. *Free Radic Biol Med*. 2007;43(6):861–8.
78. Nakayama Y, Mukai N, Kreitzer G, Patwari P, Yoshioka J. Interaction of ARRD4 With GLUT1 mediates metabolic stress in the ischemic heart. *Circ Res*. 2022;131(6):e150–27. <https://doi.org/10.1161/CIRCRESAHA.122.321351>.
79. Kalfon R, Koren L, Aviram S, Schwartz O, Hai T, Aronheim A. ATF3 expression in cardiomyocytes preserves homeostasis in the heart and controls peripheral glucose tolerance. *Cardiovasc Res*. 2017;113(2):134–46.
80. Houston-Ludlam GA, Belew AT, El-Sayed NM. Comparative transcriptome profiling of human foreskin fibroblasts infected with the Sylvio and Y Strains of *Trypanosoma cruzi*. *PLoS ONE*. 2016;11(8):e0159197. <https://doi.org/10.1371/journal.pone.0159197>.
81. Ago T, Liu T, Zhai P, Chen W, Li H, Molkentin JD, et al. A redox-dependent pathway for regulating class II HDACs and cardiac hypertrophy. *Cell*. 2008;133(6):978–93.
82. Wang J, Wang XJ, Zhang Y, Shi WJ, Lei ZD, Jiao XY. TXNIP knockout improves cardiac function after myocardial infarction by promoting angiogenesis and reducing cardiomyocyte apoptosis. *Cardiovasc Diagn Ther*. 2022;12(3):289–304.
83. Ku HC, Cheng CF. Master regulator activating transcription factor 3 (ATF3) in metabolic homeostasis and cancer. *Front Endocrinol*. 2020;14(11):552603.
84. Chen SC, Liu YC, Shyu KG, Wang DL. Acute hypoxia to endothelial cells induces activating transcription factor 3 (ATF3) expression that is mediated via nitric oxide. *Atherosclerosis*. 2008;201(2):281–8.
85. Nguyen CT, Kim EH, Luong TT, Pyo S, Rhee DK. TLR4 mediates pneumolysin-induced ATF3 expression through the JNK/p38 pathway in *Streptococcus pneumoniae*-infected RAW 264.7 cells. *Mol Cells*. 2015;38(1):58–64.
86. Garcia-Silva MR, Cabrera-Cabrera F, Das Neves RFC, Souto-Padrón T, De Souza W, Cayota A. Gene Expression changes induced by trypanosoma cruzi shed microvesicles in mammalian host cells: relevance of tranderived halves. *Biomed Res Int*. 2014;2014:1–11.
87. Hoetzenecker W, Echtenacher B, Guenova E, Hoetzenecker K, Woelbing F, Brück J, et al. ROS-induced ATF3 causes susceptibility to secondary infections during sepsis-associated immunosuppression. *Nat Med*. 2011;18(1):128–34.
88. Soraya AS, Tali H, Rona S, Tom F, Roy K, Ami A. ATF3 expression in cardiomyocytes and myofibroblasts following transverse aortic constriction displays distinct phenotypes. *IJC Heart Vasc*. 2021;1(32):100706.
89. Koren L, Elhanani O, Kehat I, Hai T, Aronheim A. Adult cardiac expression of the activating transcription factor 3, ATF3, promotes ventricular hypertrophy. *PLoS ONE*. 2013;8(7):e68396. <https://doi.org/10.1371/journal.pone.0068396>.
90. Dumoulin PC, Burleigh BA. Stress-induced proliferation and cell cycle plasticity of intracellular *Trypanosoma cruzi* amastigotes. *MBio*. 2018. <https://doi.org/10.1128/mbio.00673-18>.
91. Wesseling M, de Poel JHC, de Jager SCA. Growth differentiation factor 15 in adverse cardiac remodelling: from biomarker to causal player. *ESC Heart Fail*. 2020;7(4):1488.
92. Heeger J, Schiegnitz E, von Waldhausen D, Anwar MM, Piper HM, Euler G. Growth differentiation factor 15 acts anti-apoptotic and pro-hypertrophic in adult cardiomyocytes. *J Cell Physiol*. 2010;224(1):120–6.
93. Xu J, Kimball TR, Lorenz JN, Brown DA, Bauskin AR, Klevitsky R, et al. GDF15/MIC-1 functions as a protective and antihypertrophic factor released from the myocardium in association with SMAD protein activation. *Circ Res*. 2006;98(3):342–50. <https://doi.org/10.1161/01.RES.0000202804.84885.d0>.
94. Zingales B, Miles MA, Campbell DA, Tibayrenc M, Macedo AM, Teixeira MMG, et al. The revised *Trypanosoma cruzi* subspecific nomenclature: rationale, epidemiological relevance and research applications. *Infect Genet Evol*. 2012;12(2):240–53.
95. Poveda C, Fresno M, Ria Gironè SN, Martins-Filho OA, David Ramírez J, Santi-Rocca J, et al. Cytokine profiling in Chagas disease: towards understanding the association with infecting *Trypanosoma cruzi* discrete typing units (A BENEFIT TRIAL Sub-Study). www.plosone.org. Accessed 26 Dec 2022.
96. Velásquez-Ortiz N, Herrera G, Hernández C, Muñoz M, Ramírez JD. Discrete typing units of *Trypanosoma cruzi*: geographical and biological distribution in the Americas. *Sci Data*. 2022. <https://doi.org/10.1038/s41597-022-01452-w>.
97. Brenière SF, Waleckx E, Barnabé C. Over six thousand *Trypanosoma cruzi* strains classified into discrete typing units (dtus): attempt at an inventory. *PLoS Negl Trop Dis*. 2016;10(8):e0004792.
98. Macedo AM, Segatto M. Implications of *Trypanosoma cruzi* intraspecific diversity in the pathogenesis of chagas disease. *Am Trypanos*. 2010;1:489–522.
99. Jiménez P, Jaimes J, Poveda C, Ramírez JD. A systematic review of the *Trypanosoma cruzi* genetic heterogeneity, host immune response and genetic factors as plausible drivers of chronic Chagas cardiomyopathy. *Parasitology*. 2019;146(3):269–83.
100. Queiroga TBD, de Pereira NS, da Silva DD, de Andrade CM, de Júnior RFA, do Brito CRN, et al. Virulence of *Trypanosoma cruzi* strains is related to the differential expression of innate immune receptors in the heart. *Front Cell Infect Microbiol*. 2021;11:640.
101. Rodríguez HO, Guerrero N, Fortes A, Santi-Rocca J, Girones N, Fresno M. *Trypanosoma cruzi* strains belonging to distinct DTU causes different myocarditis patterns in infected mice. *Acta Trop*. 2014;139:57–66.
102. Ramírez JD, Guhl F, Rendón LM, Rosas F, Marin-Neto JA, Morillo CA. Chagas cardiomyopathy manifestations and *Trypanosoma cruzi* genotypes circulating in chronic Chagasic patients. *PLoS Negl Trop Dis*. 2010;4(11):e899.
103. Nielebock MAP, Moreira OC, das Xavier SCC, de Miranda LFC, de Lima ACB, de Pereira TOJS, et al. Association between *Trypanosoma cruzi* DTU TcII and chronic Chagas disease clinical presentation and outcome in an urban cohort in Brazil. *PLoS ONE*. 2020;15(12):e0243008.
104. de Oliveira MT, Fuzo CA, da Silva MC, Donadi EA, da Silva JS, Moreira HT, et al. Correlation of TcII discrete typing units with severe chronic Chagas cardiomyopathy in patients from various Brazilian geographic regions. *PLoS Negl Trop Dis*. 2022;16(12):e0010713. <https://doi.org/10.1371/journal.pntd.0010713>.
105. Burgos JM, Diez M, Vigliano C, Bisio M, Rizzo M, Duffy T, et al. Molecular identification of *Trypanosoma cruzi* discrete typing units in end-stage chronic Chagas heart disease and reactivation after heart transplantation. *Clin Infect Dis*. 2010;51(5):485–95.

106. Sykes ML, Kennedy EK, Avery VM. Impact of laboratory-adapted intracellular *Trypanosoma cruzi* strains on the activity profiles of compounds with anti-*T. cruzi* activity. *Microorganisms*. 2023;11(2):476.
107. Benatar AF, García GA, Bua J, Cerliani JP, Postan M, Tasso LM, et al. Galectin-1 prevents infection and damage induced by *Trypanosoma cruzi* on cardiac cells. *PLoS Negl Trop Dis*. 2015;9(10):e0004148. <https://doi.org/10.1371/journal.pntd.0004148>.

Publisher's Note

Springer Nature remains neutral with regard to jurisdictional claims in published maps and institutional affiliations.

Ready to submit your research? Choose BMC and benefit from:

- fast, convenient online submission
- thorough peer review by experienced researchers in your field
- rapid publication on acceptance
- support for research data, including large and complex data types
- gold Open Access which fosters wider collaboration and increased citations
- maximum visibility for your research: over 100M website views per year

At BMC, research is always in progress.

Learn more biomedcentral.com/submissions

